ACS APPLIED MATERIALS & INTERFACES

Research Article

www.acsami.org

Efficient CO_2 Capture by Functionalized Graphene Oxide Nanosheets as Fillers To Fabricate Multi-Permselective Mixed Matrix Membranes

Xueqin Li,[†,‡] Youdong Cheng,[†] Haiyang Zhang,[†,‡] Shaofei Wang,[†,‡] Zhongyi Jiang,[†,‡] Ruili Guo,[∥] and Hong Wu*[,†,‡,§]

[†]Key Laboratory for Green Chemical Technology of Ministry of Education, School of Chemical Engineering and Technology, Tianjin University, Tianjin 300072, China

[‡]Collaborative Innovation Center of Chemical Science and Engineering (Tianjin), Tianjin 300072, China

[§]Tianjin Key Laboratory of Membrane Science and Desalination Technology, Tianjin University, Tianjin 300072, China

[∥]Key Laboratory for Green Process of Chemical Engineering of Xinjiang Bingtuan, School of Chemistry and Chemical Engineering, Shihezi University, Xinjiang, Shihezi 832003, China

ABSTRACT: A novel multi-permselective mixed matrix membrane (MP-MMM) is developed by incorporating versatile fillers functionalized with ethylene oxide (EO) groups and an amine carrier into a polymer matrix. The as-prepared MP-MMMs can separate CO_2 efficiently because of the simultaneous enhancement of diffusivity selectivity, solubility selectivity, and reactivity selectivity. To be specific, MP-MMMs were fabricated by incorporating polyethylene glycol- and polyethylenimine-functionalized graphene oxide nanosheets (PEG−PEI−GO) into a commercial low-cost Pebax matrix. The PEG−PEI−GO plays multiple roles in enhancing membrane performance. First, the high-aspect ratio GO nanosheets in a polymer matrix increase the length of the tortuous path of gas diffusion and generate a rigidified interface between the polymer matrix and fillers, enhancing the diffusivity selectivity. Second, PEG consisting of EO groups has excellent affinity for CO_2 to enhance the solubility selectivity. Third, PEI with abundant primary, secondary, and tertiary amine groups reacts reversibly with CO_2 to enhance reactivity selectivity. Thus, the as-prepared MP-MMMs exhibit excellent CO_2 permeability and CO_2/gas selectivity. The MP-MMM doped with 10 wt % PEG−PEI−GO displays optimal gas separation performance with a CO_2 permeability of 1330 Barrer, a CO_2/CH_4 selectivity of 45, and a CO_2/N_2 selectivity of 120, surpassing the upper bound lines of the Robeson study of 2008 (1 Barrer = 10^{-10} cm^3 (STP) cm^{-2} s^{-1} cm^{-1} Hg).

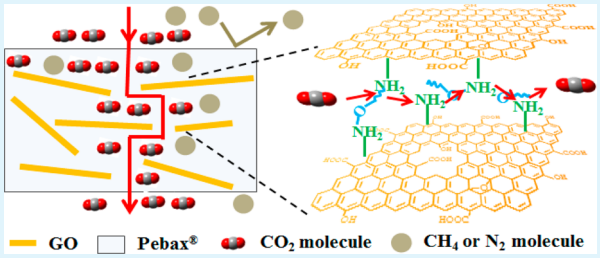

1. INTRODUCTION

Membrane technology has shown great potential in CO_2 capture from economic and environmental perspectives.[1−3] Mixed matrix membranes (MMMs) consisting of a polymer as the continuous phase and an inorganic filler as the dispersed phase[4] can potentially overcome Robeson's upper bound trade-off limit.[5,6] The fillers embedded in the polymer matrix are classified into conventional fillers (zeolites, silicas, and metal oxides) and alternative fillers [carbon nanotubes (CNTs), metal organic frameworks (MOFs), and graphenes].[7−17] These fillers provide the possibility of improved development of high-performance membranes with the aid of the properties and functionalization of fillers.

Graphene oxide (GO) is a good candidate as a nanofiller in MMMs because of its high aspect ratio (>1000), easy surface functionalization, and high thermal and mechanical properties.[18,19] The high-aspect ratio fillers increase the length of the tortuous path of gas diffusion in the polymer matrix and reduce the mobility of polymer chains. This will restrict the diffusion of larger molecules but favor the diffusion of small molecules with less resistance, thus improving gas diffusivity selectivity.[20−25] Because ethylene oxide (EO) groups possess excellent affinity for polar gases like CO_2, the introduction of EO groups into membranes can achieve high CO_2/gas selectivity because of the increase in solubility selectivity.[26−29] In addition, CO_2 is an acidic gas, and basic groups such as amine groups are widely used as CO_2 carriers. The reactivity selectivity of membranes is enhanced by increasing the content of amino groups due to the reversible reactions between CO_2 and amine groups.[30−34] The reactions between CO_2 and amino groups in the presence of water were reported as follows:

$$2CO_2 + 2RNH_2 + H_2O \leftrightarrow RNHCOOH + RNH_3^+ + HCO_3^- \quad (1)$$

$$2CO_2 + 2RR'NH + H_2O \leftrightarrow RR'NCOOH + RR'NH_2^+ + HCO_3^- \quad (2)$$

$$CO_2 + RR'R''N + H_2O \leftrightarrow RR'R''NH^+ + HCO_3^- \quad (3)$$

Received: January 6, 2015
Revised: February 12, 2015
Published: February 16, 2015

© 2015 American Chemical Society

DOI: 10.1021/acsami.5b00106
ACS Appl. Mater. Interfaces 2015, 7, 5528−5537

where R, R′, and R″ may be the same organic group or different organic groups.

For example, Ismail et al.[20] found that the incorporation of layered silicate into the polymer matrix can increase diffusivity selectivity, because high-aspect ratio fillers in the polymer matrix increased the length of the tortuous path for the diffusion of larger molecules. Filiz et al.[27] incorporated PEG-functionalized polyoctahedral oligomeric silsesquioxanes (POSS) into a poly(ether-*block*-amide) (Pebax) matrix and found that the solubility of CO_2 increased with increasing PEG−POSS loading because of the excellent affinity between EO and CO_2. Wang et al.[35] fabricated composite membranes containing polyaniline nanorods, and CO_2 molecules could transfer quickly because of the reversible reaction with amino groups. In our previous work,[36] we incorporated amine-functionalized mesoporous silica into the Pebax matrix and found that abundant amine groups can efficiently facilitate CO_2 transport by a reversible reaction.

As mentioned above, the conventional strategies mainly focus on the improvement of gas separation performance by enhancing a single permselectivity, such as diffusivity selectivity, solubility selectivity, or reactivity selectivity;[37−39] however, the improvement of membrane performance is always limited. To overcome the limitations, we proposed a novel concept for fabricating multi-permselective mixed matrix membranes (MP-MMMs) by combining diffusivity selectivity, solubility selectivity, and reactivity selectivity. On the basis of the differences between CO_2 and other gases (CH_4 or N_2) in size, condensability, and reactivity, diffusivity selectivity can be enhanced by incorporating high-aspect ratio fillers, solubility selectivity can be enhanced by introducing EO groups, which have excellent affinity for CO_2, and reactivity selectivity can be enhanced by introducing amine carriers that react reversibly with CO_2.

In this study, MP-MMMs were fabricated by incorporating GO nanosheets functionalized with polyethylene glycol monomethyl ether (PEG, EO groups) and polyethylenimine (PEI, amine carrier) into a commercial low-cost Pebax matrix. The objective of this study was to simultaneously enhance the diffusivity selectivity, solubility selectivity, and reactivity selectivity of membranes. The essence of our discovery is embodied mainly in the following experiments. The physical properties of the membranes in terms of microstructure, thermal stability. and crystallization were investigated; moreover, the effects of functionalized GO on solubility selectivity, diffusivity selectivity, and reactivity selectivity were systematically examined.

2. EXPERIMENTAL SECTION

2.1. Materials. Pebax MH 1657 (Scheme 1) was purchased from Shanghai Rongtian Chemical Co., Ltd. Natural graphite flake (2500 mesh) was purchased from Qingdao Tianhe Graphite Co. Ltd. Branched polyethylenimine (PEI; M_w = 20 kDa) was purchased from Cheng du Geleixiya Chemical Technology Co., Ltd. Polyethylene glycol monomethyl ether (PEG; M_w = 5 kDa), 1-ethyl-3-[3-(dimethylamino)propyl]carbodiimide hydrochloride (EDC), *N*-hydroxysuccinimide (NHS), thionyl chloride ($SOCl_2$, 99.7%), and pyridine (Py, 99.9%) were purchased from Aladdin Chemistry Co. Ltd. 1,1′-Carbonyldiimidazole (CDI) was purchased from Heowns Biochemical Technologies Co., Ltd. The dialysis bag [molecular weight cutoffs (MWCOs) of 3.5 and 10 kDa] was purchased from Beijing Rui Da Heng Hui Science & Technology Development Co., Ltd. Concentrated sulfuric acid (H_2SO_4, 98 wt %), hydrochloric acid (HCl), and potassium permanganate ($KMnO_4$) were purchased from Tianjin Kewei Ltd. A hydrogen peroxide aqueous solution (H_2O_2, 30 wt %), sodium nitrate ($NaNO_3$), and *N*,*N*-dimethylformamide (DMF, 99.5 wt %) were purchased from Tianjin Guangfu Technology Development Co. Ltd. (Tianjin, China). All the reagents were of analytical grade and used without further purification. Deionized water from a Millipore system (Milli-Q) was used in all experiments.

Scheme 1. Chemical Structures of (a) Pebax MH 1657, (b) PEI, and (c) PEG

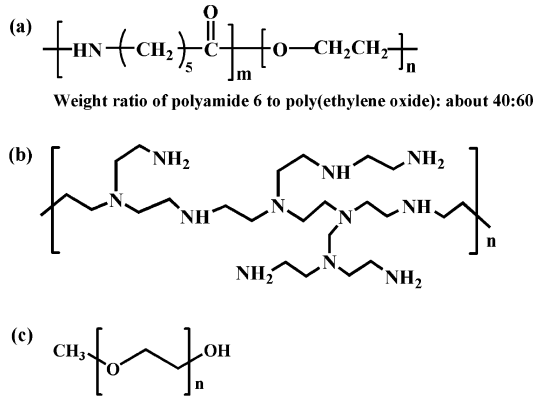

2.2. Preparation of PEG−PEI−GO Nanofillers. Graphene oxide was synthesized by a modified Hummers method.[40] Graphite powder (5.0 g) and $NaNO_3$ (2.5 g) were dissolved in concentrated H_2SO_4 (115 mL) while the mixture was being stirred in an ice bath. Then $KMnO_4$ (15.0 g) was added slowly to the mixture while the mixture was being stirred for 2 h while the temperature was kept below 5 °C. The temperature was increased to 35 ± 2 °C and the mixture vigorously stirred for 30 min. Next, 230 mL of distilled water was added to the mixture while the temperature was kept below 100 °C. Finally, 20 mL of H_2O_2 was added dropwise. The mixture was filtered and washed with 250 mL of an aqueous HCl solution (1:10 HCl:H_2O) to remove metal ions. Then the mixture was centrifuged and washed with large amounts of water until the filtrate was neutral. The final product was obtained by centrifugation to remove the large and not fully exfoliated parts.

The schematic illustration of the preparation of PEG−PEI−GO is shown in Scheme 2. To prepare the PEI−GO, a 0.5 mg/mL GO solution was sonicated for 1 h; 54.3 mg/mL EDC and 50.6 mg/mL NHS were then added to the GO solution. PEI was then added to the

Scheme 2. Illustration of the Preparation of PEG−PEI−GO

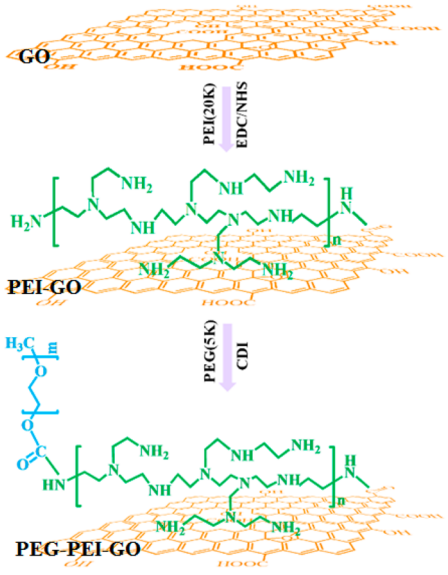

DOI: 10.1021/acsami.5b00106
ACS Appl. Mater. Interfaces 2015, 7, 5528−5537

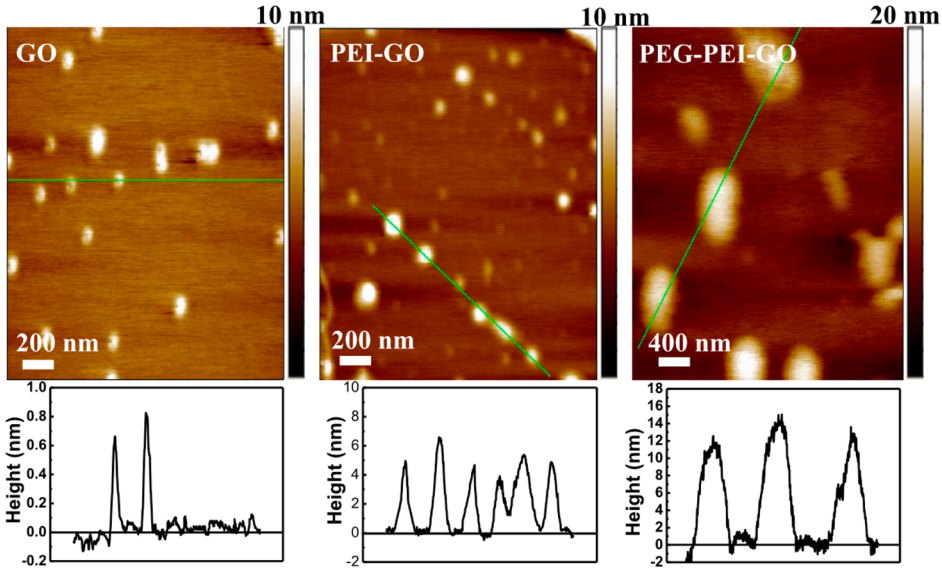

Figure 1. AFM images of GO, PEI−GO, and PEG−PEI−GO.

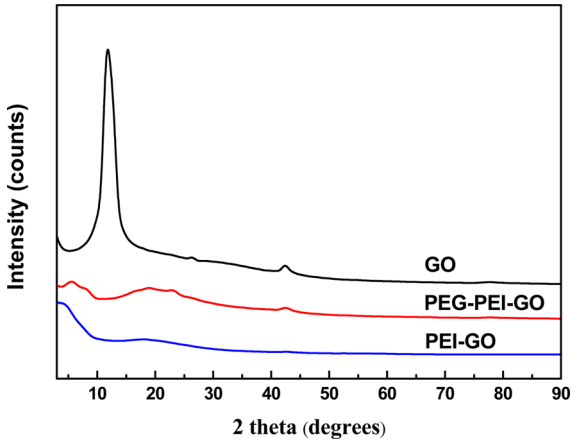

Figure 2. XRD patterns of GO, PEI−GO, and PEG−PEI−GO.

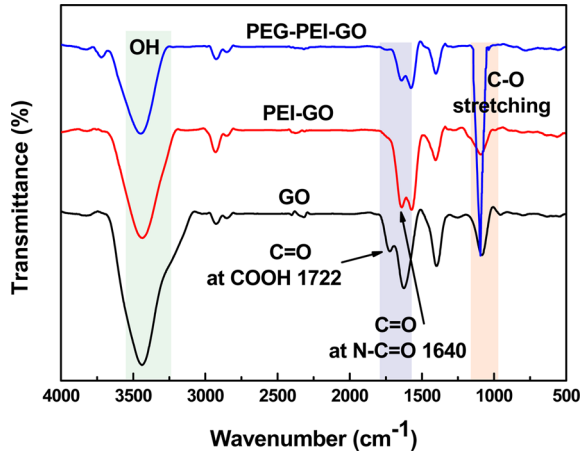

Figure 3. FT-IR spectra of GO, PEI−GO, and PEI−PEG−GO.

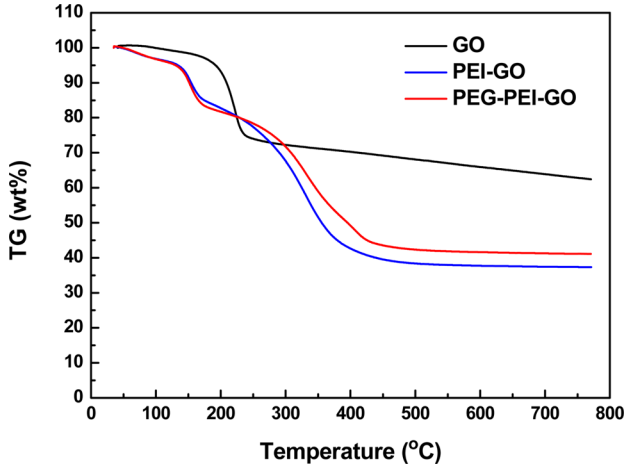

Figure 4. TGA curves of GO, PEI−GO, and PEI−PEG−GO.

mixture, and the weight ratio of PEI to GO was 5:1. After being sonicated for 5 min, the solution was stirred for 1 day at room temperature. The resulting PEI−GO mixture was dialyzed against deionized water using a MWCO 3500 dialysis bag for 2 days to remove the unreacted PEI.

To prepare the PEG−PEI−GO, 0.5 mg/mL PEI-GO was sonicated for 1 h, the activated PEG was added to the solution, and the weight ratio of PEG to GO was 2:1. The mixture was stirred at room temperature for 12 h; after that, the mixture was dialyzed by a MWCO 10000 dialysis bag. Then the obtained PEG−PEI−GO fillers were dried at 50 °C in a vacuum oven for 3 days. The activated PEG was prepared as follows. PEG (1 g/mL) was dissolved in anhydrous DCM, and then CDI was added to the PEG solution to reach a concentration of ∼0.03 g/mL. The mixture suspension was reacted overnight under a nitrogen atmosphere at room temperature. The solvent was evaporated using a rotary evaporator, precipitated by addition of ice-cold diethyl ether, and dried under vacuum.

To prepare PEG−GO, a 20 mg/mL GO/DMF solution was sonicated to obtain a stably dispersed GO solution. The stable suspension of GO/DMF was refluxed in a 5 mg/mL GO/$SOCl_2$ solution at 70 °C for 24 h, and the excess of $SOCl_2$ was removed by distillation. A 0.4 g/mL PEG/Py solution was added to the resulting mixture. The mixture was reacted at 120 °C for 3 days while being stirred. The suspension was filtered, and the resulting PEG−GO was dried at 40 °C under vacuum.

2.3. Membrane Preparation. MP-MMMs and a pristine Pebax membrane were prepared by a solution-casting method. To prepare a 4 wt % solution of Pebax, 0.8 g Pebax pellets were dissolved in a solvent mixture of 70 wt % ethanol and 30 wt % water under reflux

DOI: 10.1021/acsami.5b00106
ACS Appl. Mater. Interfaces 2015, 7, 5528−5537

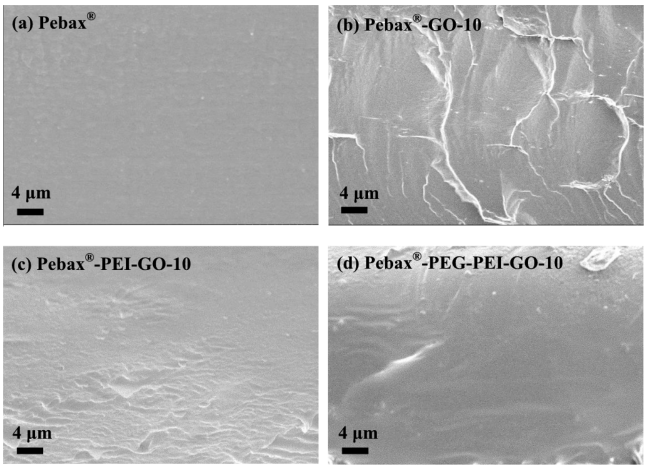

Figure 5. Comparison of cross-section SEM images of (a) pristine Pebax, (b) Pebax−GO−10, (c) Pebax−PEI−GO−10, and (d) Pebax−PEG−PEI−GO−10 membranes.

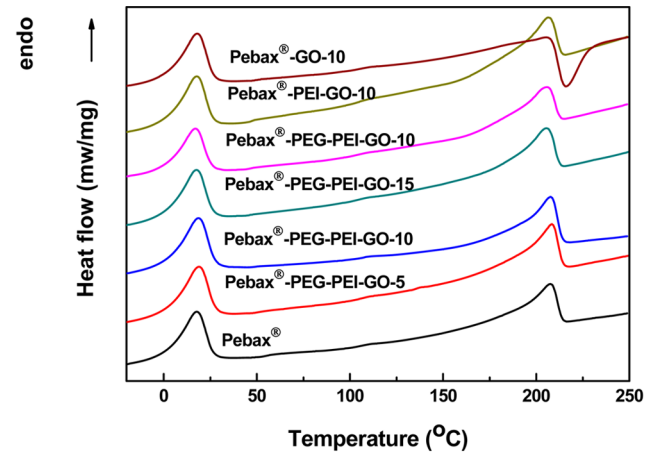

(a)

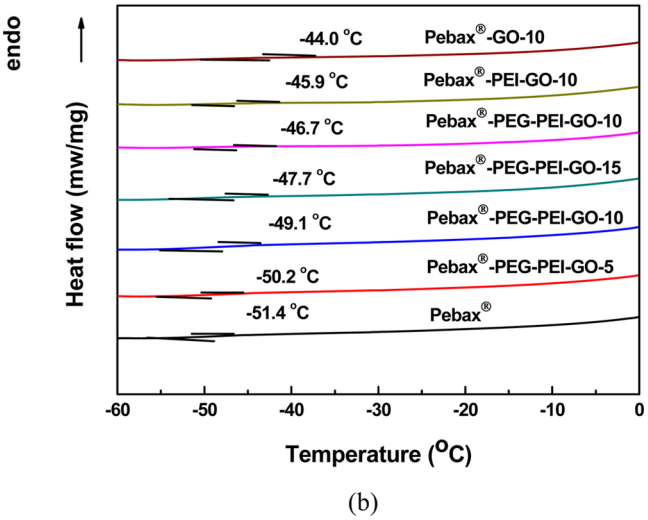

(b)

Figure 6. DSC curves of the pristine Pebax membrane, MMMs, and MP-MMMs: (a) high-temperature zone and (b) low-temperature zone.

(80 °C) for 2 h. PEG−PEI−GO was sonicated for 30 min in the Pebax solution described above. The mixture was stirred for an additional 2 h followed by being cast on a flat glass plate. The obtained membrane

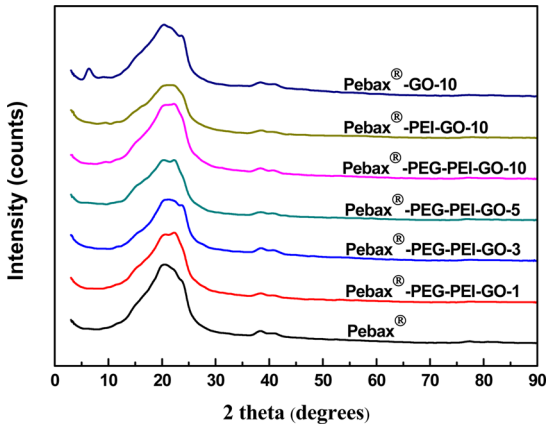

Figure 7. XRD patterns of the pristine Pebax membrane, MMMs, and MP-MMMs.

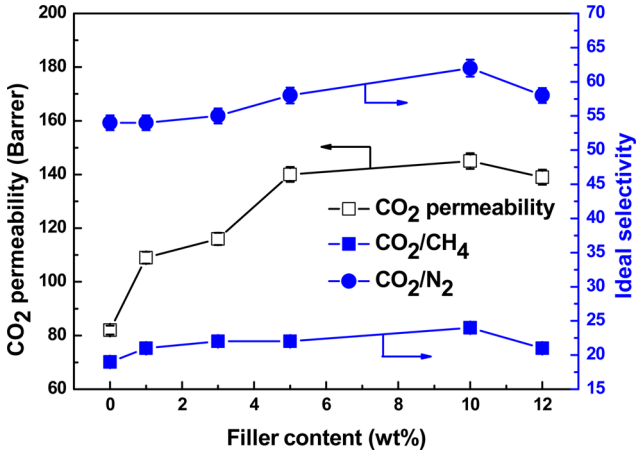

Figure 8. Effect of PEG−PEI−GO content on gas separation performance.

was air-dried at ambient temperature for 24 h. To remove the solvent residue, the membrane was dried in a vacuum oven for an additional 24 h. The pristine Pebax membrane was fabricated via the same method. The as-prepared MMMs containing PEG−PEI−GO (PEI−GO or GO) were denoted as Pebax−PEG−PEI−GO−*X* (Pebax−PEI−GO−*X* or Pebax−GO−*X*), where *X* refers to the weight percentage of PEG−PEI−GO (PEI−GO or GO) relative to the weight of the Pebax matrix. All membrane thicknesses were approximately 40−70 μm.

2.4. Membrane Characterization. *2.4.1. Atomic Force Microscope (AFM).* The size and morphology of GO, PEI−GO, and PEG−PEI−GO were investigated with an Agilent model 5500 AFM.

2.4.2. Fourier Transform Infrared (FT-IR) Spectrometer. FT-IR spectra of GO, PEI−GO, PEG−PEI−GO, and membranes were measured using a BRUKER Vertex 70 FT-IR spectrometer in the range of 4000−400 cm^{-1}. Before FT-IR measurement, the membrane sample was contacted with pure CO_2 for several hours to reach the sorption equilibrium. To desorb CO_2, the membrane was placed in the air for several hours to reach the desorption equilibrium.

2.4.3. Elemental Analyzer (EA). Elemental analysis data of GO, PEI−GO, and PEG−PEI−GO were obtained by an vario EL CUBE EA.

2.4.4. Thermogravimetric Analyses (TGAs). TGA of GO, PEI−GO, and PEG−PEI−GO was performed using a NETZSCH TG 209 F3 thermal analyzer. The data were recorded at a heating rate of 10 °C/min from 30 to 800 °C in a nitrogen atmosphere.

2.4.5. Differential Scanning Calorimeter (DSC). The thermal properties and glass transition temperatures (T_g) of membranes were measured with a DSC using a NETZSCH DSC 200 F3 thermal

DOI: 10.1021/acsami.5b00106
ACS Appl. Mater. Interfaces 2015, 7, 5528−5537

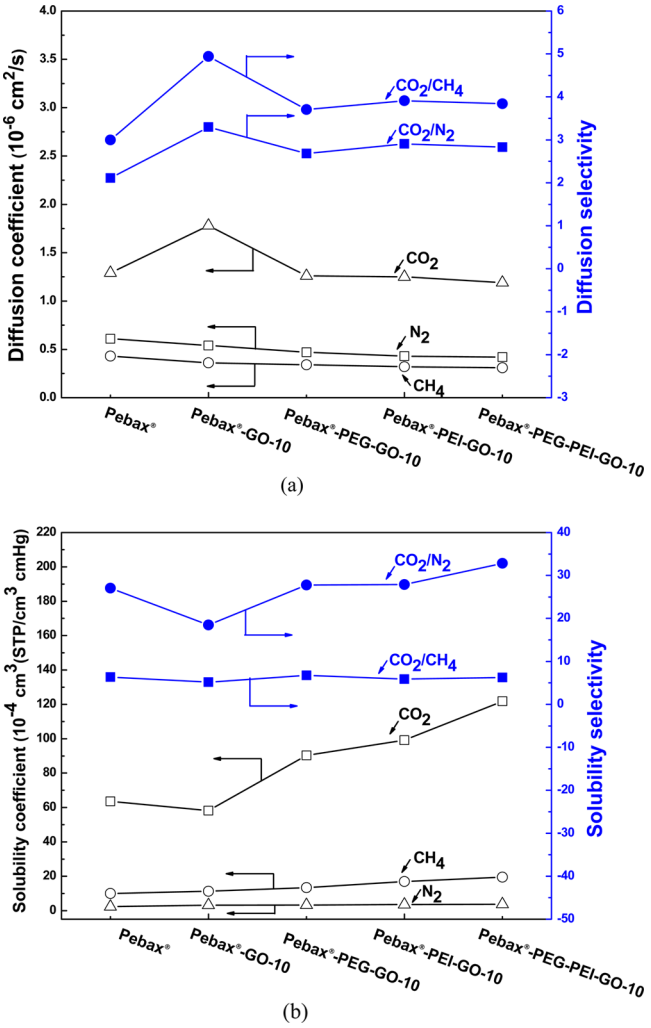

Figure 9. (a) Diffusivity and (b) solubility of gases in dry membranes.

analyzer at a heating rate of 10 °C/min in the temperature range of 60−250 °C under a nitrogen atmosphere.

2.4.6. X-ray Diffraction (XRD). A Rigaku D/max 2500 v/pc power X-ray diffractometer was used to obtain the solid state structure of fillers. The diffraction data of fillers were recorded in the range of 3−90° at a scan rate of 2°/min. The membranes were assessed using 2θ angles between 3° and 90° at a scan rate of 10°/min. The average d spacing of the Pebax matrix was evaluated on the basis of Bragg's law.[41]

2.4.7. Scanning Electron Microscope (SEM). The cross-sectional morphologies of the pristine Pebax membrane, MMMs, and MP-MMMs were examined by a Nanosem 430 SEM.

2.5. Gas Permeation Experiments. Both pure- and mixed-gas (30:70 CO_2/CH_4, 10:90 CO_2/N_2, volume percent) permeation experiments were conducted using the conventional constant-pressure/variable-volume method as described previously.[42] The membranes was measured under dry or humidified conditions. In the humidified permeation experiments, the feed gas was saturated with water vapor by bubbling through a water bottle at 35 °C and then passing an empty bottle at room temperature (25 °C) to remove the condensate water. The sweep gas was also humidified by being passed through water bubblers at room temperature. The detailed experimental apparatus and procedure were described in our previous work.[36] Gas permeability [P_i, Barrer, and 1 Barrer = 10^{-10} cm^3 (STP) cm/(cm^2 s cmHg)] under steady state was determined by the following equation:

$$P_i = \frac{Q_i l}{\Delta P_i A} \tag{4}$$

where Q_i signifies the volumetric flow rate of gas i [cm^3 (STP/s)], l refers to the membrane thickness (cm), Δp_i is the transmembrane partial pressure difference of gas i (cmHg), and A represents the effective membrane area (12.56 cm^2). The CO_2/CH_4 (or CO_2/N_2) selectivities (α_{ij}) were calculated from the ratio of the permeabilities of the gases:

$$\alpha_{ij} = \frac{P_i}{P_j} \tag{5}$$

where P_i and P_j denote the permeability of gases i and j, respectively.

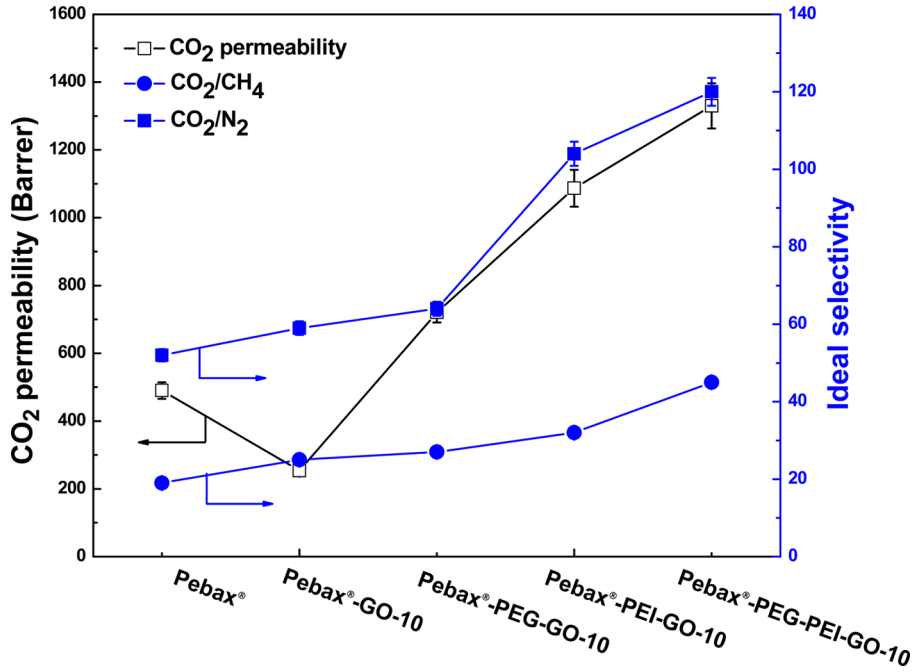

Figure 10. Pure gas permeability and ideal selectivity of the humidified membranes.

DOI: 10.1021/acsami.5b00106
ACS Appl. Mater. Interfaces 2015, 7, 5528−5537

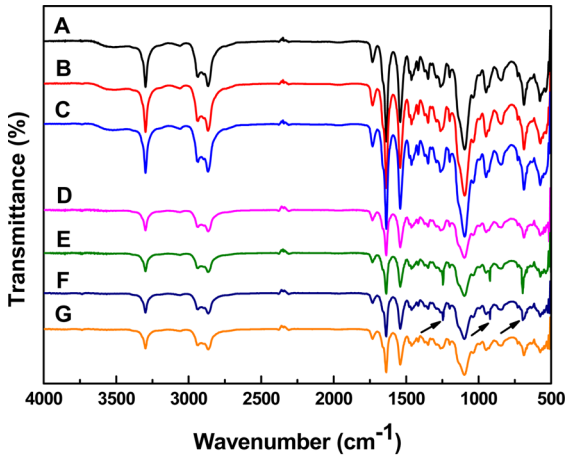

(a)

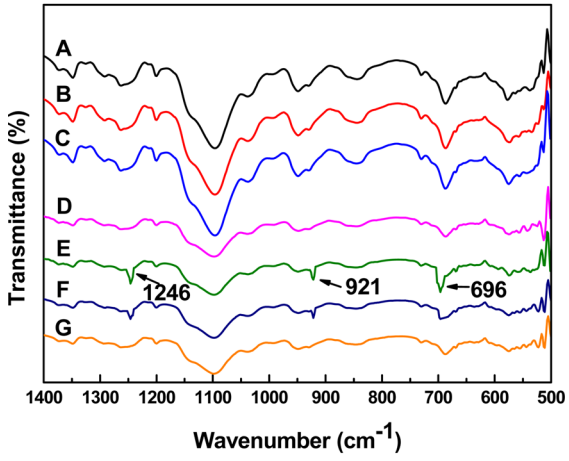

(b)

Figure 11. FT-IR spectra of (a) CO_2 adsorption and desorption within membranes (4000−500 cm^{-1}) and (b) amplification of the low-wavenumber zone (1400−500 cm^{-1}): (A) pristine Pebax membrane, (B) CO_2-absorbed pristine Pebax membrane, (C) CO_2-desorbed pristine Pebax membrane, (D) Pebax−PEG−PEI−GO membrane, (E) CO_2-absorbed Pebax−PEG−PEI−GO membrane, (F) CO_2-desorbed Pebax−PEG−PEI−GO membrane (20 min), and (G) CO_2-desorbed Pebax−PEG−PEI−GO membrane (6 h).

Because the permeate side is kept at ambient pressure, the mixed-gas separation factor could also be calculated by eq 5.

The diffusion, permeability, and solubility of membranes for pure gases were measured by the "time-lag" method.[43] The feed pressure and temperature were kept at 2 bar and 30 °C, respectively. The measurement was conducted three times for each membrane.

3. RESULTS AND DISCUSSION

3.1. Nanofiller Characterization. The size and morphology of GO, PEI−GO, and PEG−PEI−GO were characterized by an AFM, as shown in Figure 1. The size and thickness of the unmodified GO nanosheets are approximately 80−250 and 0.6−0.9 nm, respectively. After the functionalization, the size of PEI−GO changes slightly and the thickness of PEI−GO increases to ∼5 nm. The size of PEG−PEI−GO increases to 400−800 nm, and the thickness of PEG−PEI−GO increases to ∼13 nm. The increase in the thickness of both PEI−GO and PEG−PEI−GO suggests that PEI and PEG are successfully conjugated to GO nanosheets.

XRD patterns of GO, PEI−GO, and PEG−PEI−GO are displayed in Figure 2. The XRD pattern of GO nanosheets has a strong peak at a 2θ of 11.6°, corresponding to a (001) reflection and a d spacing of 0.76 nm. Compared to the pattern of GO nanosheets, the strong diffraction peaks in XRD patterns of both PEI−GO and PEG−PEI−GO disappear at 11.6° and a broad diffuse peak is exhibited at ∼20°. The broad peak indicates that the functionalized GO nanosheets are in a disordered state and poorly ordered along the different stacking directions. This may arise from the introduction of PEI and PEG onto GO nanosheets.

As shown in Figure 3, FT-IR spectra of PEI−GO and PEI−PEG−GO reveal the presence of a new peak at 1640 cm^{-1} corresponding to an amide bond in comparison with the spectrum of unmodified GO. This infers that PEI is covalently conjugated to the carboxylic group of GO. The band at 1093 cm^{-1} suggests the presence of C−O stretching in PEG, confirming the introduction of PEG onto GO nanosheets.

The PEI contents in PEG−PEI−GO and PEI−GO were measured by elementary analysis to be 33 and 38%, respectively. The PEG content in PEG−PEI−GO was estimated to be 20.9% using TGA as shown in Figure 4.

3.2. Membrane Characterization. As shown in Figure 5, SEM micrographs reveal the internal microstructure of the membranes. Figure 5b presents a wrinkled cross section because the unmodified GO nanosheets are poorly distributed in the polymer matrix and have poor compatibility with the polymer matrix. The cross-section SEM images (Figure 5c,d) become smooth, and no voids form in MMMs doped with functionalized GO. It indicated that PEG and PEI on the surface of GO improve the interface compatibility between the Pebax matrix and GO nanosheets.

Figure 6 shows DSC curves of a pristine Pebax membrane, MMMs, and MP-MMMs. For the pristine Pebax membrane, two endothermic peaks observed at 17 and 208 °C are attributed to the melting temperature of the polyether block and polyamide block, respectively. MMMs doped with PEI−GO and PEG−PEI-GO show the same two endothermic peaks as the pristine Pebax membrane, but MMMs doped with unmodified GO show an exothermic peak at 216 °C. The exothermic peak may result from the crystallinity of the polymer matrix in the presence of GO laminates. It is observed that glass transition temperatures (T_g) of MMMs and MP-MMMs are higher than that of the pristine Pebax membrane, indicating that the presence of fillers in the polymer matrix restricts the mobility of Pebax chains and generates a rigidified interface between the polymer and fillers. This is beneficial for improving the diffusivity selectivity of membranes.

The crystalline properties of the pristine Pebax membrane, MMMs, and MP-MMMs are measured by XRD. As shown in Figure 7, all membranes display a broad peak around a 2θ of 23°, and this broad peak results from the crystalline region of polyamide segments. MMMs doped with unmodified GO present a peak at a 2θ of 6.4°, indicating that a small fraction of GO nanosheets retain their stack structure while the majority are homogeneously dispersed into the polymer matrix. The peak at a 2θ of 6.4° becomes weaker and disappears in MP-MMMs, because the functionalized GO nanosheets are homogeneously dispersed in the polymer matrix. The average d spacing increases from 0.402 nm for the pristine Pebax membrane to 0.431 nm for the Pebax−PEG−PEI−GO−10 membrane. The increase in d spacing will improve the gas permeability of membranes.

3.3. Membrane Separation Performance. *3.3.1. Pure Gas Permeation Performance.* To investigate the effect of

DOI: 10.1021/acsami.5b00106
ACS Appl. Mater. Interfaces 2015, 7, 5528−5537

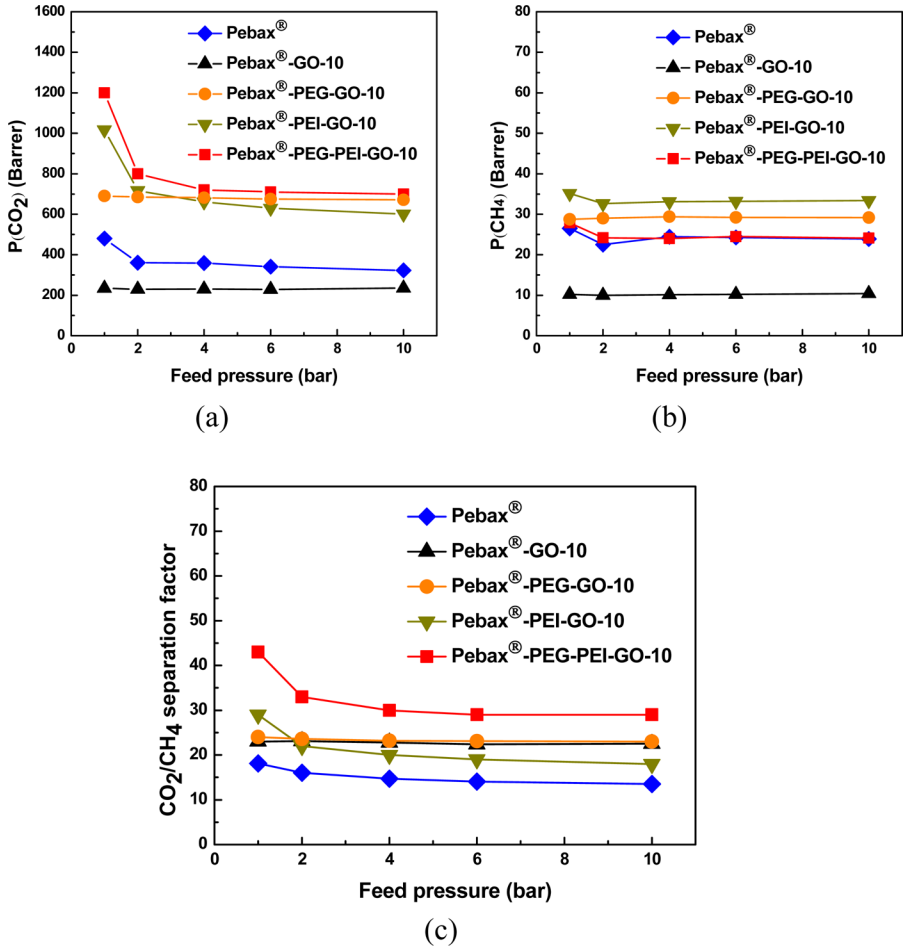

Figure 12. Variation of (a) CO_2 permeability, (b) CH_4 permeability, and (c) CO_2/CH_4 separation factor with feed pressure for pristine Pebax, Pebax−GO−10, Pebax−PEG−GO−10, Pebax−PEI−GO−10, and Pebax−PEG−PEI−GO−10 membranes.

PEG−PEI−GO loading on membrane properties, Pebax membranes were fabricated with different filler loadings. The permeability and selectivity at different PEG−PEI−GO loadings are shown in Figure 8. The CO_2 permeability, CO_2/CH_4 selectivity, and CO_2/N_2 selectivity gradually increase from 1 to 10 wt % with the increase in PEG−PEI−GO content. When the PEG−PEI−GO loading increases to 12 wt %, both CO_2 permeability and CO_2/gas selectivity decrease. MP-MMMs doped with 10 wt % PEG−PEI−GO exhibit the best performance with a CO_2 permeability of 145 Barrer, a CO_2/CH_4 selectivity of 24, and a CO_2/N_2 selectivity of 62. Herein, 10 wt % filler loading was chosen as the optimal loading in membranes for the further discussion of gas permeation properties.

To further explore the role of the fillers in the gas permeation process, the diffusivity coefficient (D) and thge solubility coefficient (S) of membranes were measured by the time-lag method.[43] The diffusion and solubility selectivities of CO_2/CH_4 and CO_2/N_2 are displayed in Figure 9. It can be seen from Figure 9a that CO_2/CH_4 and CO_2/N_2 diffusion selectivities of MMMs and MP-MMMs are higher than that of the pristine Pebax membrane. The order of gas diffusivities is closely related to kinetic diameters of gas molecules, and the kinetic diameter increases as follows: CO_2 (3.3 Å) < N_2 (3.6 Å) < CH_4 (3.8 Å).[44] The sheet structure of high-aspect ratio GO leads to the highly tortuous diffusion path in the polymer matrix and generates a rigidified interface between the polymer matrix and fillers. This would restrict the diffusion of larger molecules and favor the diffusion of small molecules with less resistance, improving gas diffusivity selectivity. Because the difference in kinetic diameters between CO_2 and CH_4 is larger than that between CO_2 and N_2, CO_2/CH_4 diffusivity selectivity is higher than CO_2/N_2 diffusivity selectivity.

Figure 9b indicates that CO_2/CH_4 and CO_2/N_2 solubility selectivities of the Pebax−PEG−GO−10 membrane are higher than those of the pristine Pebax membrane. The membranes with solubility selectivity separate gases according to their relative condensability, which is characterized by critical temperature. The critical temperatures of gases decrease in the following order: CO_2 (304.2 K) > CH_4 (190.7 K) > N_2 (126.1 K). The higher condensability has the higher solubility of the gas in the polymer matrix.[45−48] Because the critical temperature difference between CO_2 and N_2 is larger than that of CO_2 and CH_4, the CO_2/N_2 solubility selectivity is remarkably higher than the CO_2/CH_4 solubility selectivity. The increase in the solubility selectivity of the Pebax−PEG−PEI−GO−10 membrane is due to the introduction of PEG segments, consisting of EO groups, because the presence of EO groups increases the solubility of quadrupolar CO_2 over those of the other nonpolar gases (CH_4 and N_2).

Gas separation performance was investigated under a humidified state to verify reactivity selectivity exerted by amine groups in the membranes. As shown in Figure 10, MP-MMM doped with 10 wt % PEI-functionalized GO (Pebax−PEI−GO−10) has CO_2 permeability and CO_2/gas selectivity higher than

DOI: 10.1021/acsami.5b00106
ACS Appl. Mater. Interfaces 2015, 7, 5528−5537

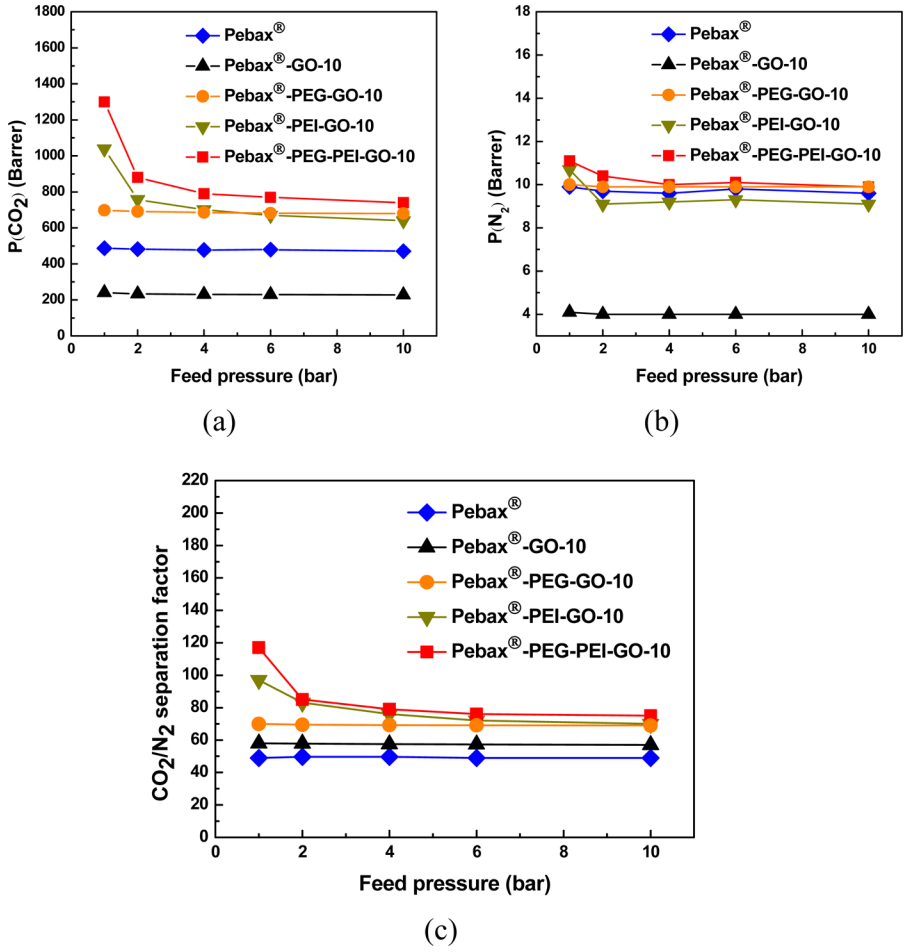

Figure 13. Variation of (a) CO_2 permeability, (b) N_2 permeability, and (c) CO_2/N_2 separation factor with feed pressure for pristine Pebax, Pebax−GO−10, Pebax−PEG−GO−10, Pebax−PEI−GO−10, and Pebax−PEG−PEI−GO−10 membranes.

those of MMM doped with 10 wt % unmodified GO (Pebax−GO−10). Because PEI is a branched polymer with abundant amine carriers, including primary amine, secondary amine, and tertiary amine groups, the specific and reversible reactions occur between CO_2 molecules and amine carriers in membranes, increasing the reactivity selectivity.

Among all membranes tested, the Pebax−PEG−PEI−GO−10 membrane presents the highest CO_2 permeability of 1330 Barrer with selectivities of 45 for CO_2/CH_4 and 120 for CO_2/N_2. Compared with the pristine Pebax membrane, the notable increments in both CO_2 permeability of ∼2.7-fold and CO_2/gas selectivity of ∼2.4-fold confirm the favorable combination effect of diffusivity selectivity, solubility selectivity, and reactivity selectivity on the membrane gas separation performance.

To confirm the possible interaction and reversible reaction between CO_2 and the membrane surface, FT-IR spectra were recorded to investigate the CO_2 adsorption and desorption behaviors on membranes.[9,49,50] The FT-IR spectra of pristine Pebax and Pebax−PEG−PEI−GO membranes after adsorbing CO_2 and desorbing CO_2 are shown in Figure 11. The pristine Pebax membrane (spectrum A), CO_2-absorbed pristine Pebax membrane (spectrum B), and CO_2-desorbed pristine Pebax membrane (spectrum C) exhibit quite similar spectra, indicating that no reactive adsorption of CO_2 happens on the pristine Pebax membrane. Compared with the Pebax−PEG−PEI−GO membrane (spectrum D), the CO_2-absorbed Pebax−PEG−PEI−GO membrane (spectrum E) shows some new peaks (indicated by arrows) in Figure 11, indicating that CO_2 reacts with the amino groups of PEI and produces carbamate salt at ∼1246 cm^{-1}. The peaks at 921 and 696 cm^{-1} are assigned to the characteristic absorption peaks of HCO_3^-. The intensity of these new peaks (spectrum F) become weaker after CO_2 is desorbed for 20 min and then disappeared (spectrum G) at desorption equilibrium. We can conclude from these FT-IR results that CO_2 can react reversibly with the Pebax−PEG−PEI−GO membrane.

3.3.2. Effect of Feed Gas Pressure. Figures 12 and 13 show gas separation performance of membranes as a function of feed pressure. As shown in Figures 12a and 13a, the CO_2 permeabilities of pristine Pebax, Pebax−GO−10, and Pebax−PEG−GO−10 membranes change slightly with an increasing feed pressure, but the permeabilities of Pebax−PEI−GO−10 and Pebax−PEG−PEI−GO−10 membranes containing amine carriers decrease significantly when the feed pressure increases from 1 to 2 bar and then decrease slightly with an increasing feed pressure. Figures 12b and 13b show an only slight decrease in CH_4 or N_2 permeability with an increasing feed pressure. This implies that only transport of CO_2 through the membrane follows mainly a facilitated transport mechanism.[51,52] The facilitated transport is based on the reversible reactions of CO_2 with amine carriers in the presence of water. In addition, the transport of CO_2 through membranes also follows a solution−diffusion mechanism, while the permeation of nonpolar CH_4 and N_2 gas molecules through the membrane follows only the

DOI: 10.1021/acsami.5b00106
ACS Appl. Mater. Interfaces 2015, 7, 5528−5537

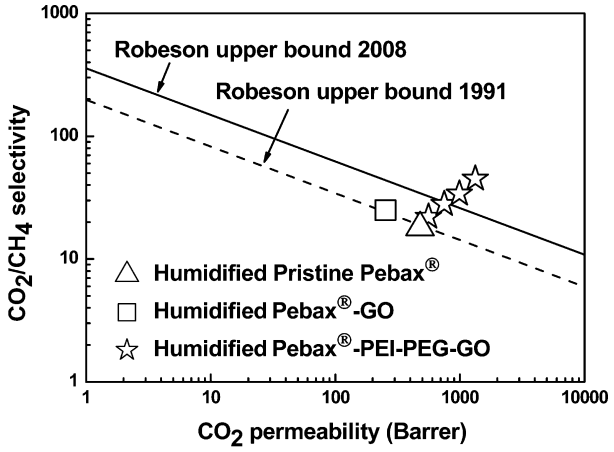

(a)

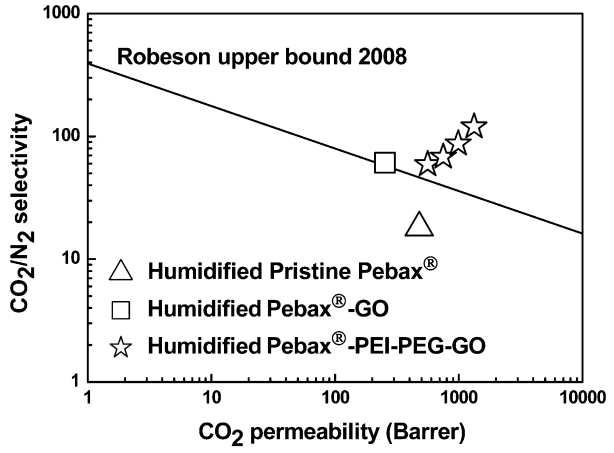

(b)

Figure 14. Robeson plots for (a) CO_2/CH_4 separation and (b) CO_2/N_2 separation.

classic solution−diffusion mechanism without facilitated transport by any reversible reactions. CO_2/CH_4 and CO_2/N_2 selectivities exhibit a decreased trend because the CO_2 permeability significantly decreases and the CH_4 or N_2 permeability slightly decreases.

3.4. Comparison of Results to Robeson's Upper Bound Curve. The permselectivities of the as-prepared membranes were also compared with Robeson's upper bound limit as illustrated in Figure 14. It is observed that MP-MMMs present the great improvements in CO_2 permeability and CO_2/gas selectivity, surpassing the 2008 Robeson upper bound limit. This further confirms that the combination of diffusivity selectivity, solubility selectivity, and reactivity selectivity in MP-MMMs is an efficient strategy for improving gas separation performance.

4. CONCLUSION

A novel multi-permselective mixed matrix membrane (MP-MMM) was successfully fabricated by incorporating versatile GO nanosheets modified by both PEG and PEI into a Pebax matrix for CO_2 capture. The permselectivity of MP-MMMs exhibits a significant increase as a comprehensive result of the simultaneous enhancement of diffusivity selectivity, solubility selectivity, and reactivity selectivity. The increase in diffusivity selectivity and solubility selectivity is confirmed by the diffusivity coefficient and solubility coefficient measured by the time-lag method. The reversible reaction between CO_2 and the membrane surface is confirmed by FT-IR results. The increase in reactivity selectivity is confirmed by the presence of amine carriers. Compared with those of the pristine Pebax membrane, the CO_2 permeability and CO_2/gas selectivity of the Pebax−PEG−PEI−GO−10 membrane increase by ∼2.7- and ∼2.4-fold, respectively. This study offers a facile and genetic strategy for the design and fabrication of membranes with multi-permselectivity to enhance the CO_2 capture property.

AUTHOR INFORMATION

Corresponding Author

*Fax: +86 22 2350 0086. Telephone: +86 22 2350 0086. E-mail: wuhong@tju.edu.cn.

Notes

The authors declare no competing financial interest.

ACKNOWLEDGMENTS

We gratefully acknowledge the support from the National High Technology Research and Development Program of China (2012AA03A611), the Program for New Century Excellent Talents in University (NCET-10-0623), the National Science Fund for Distinguished Young Scholars (21125627), and the Programme of Introducing Talents of Discipline to Universities (B06006).

REFERENCES

(1) Rezakazemi, M.; Ebadi Amooghin, A.; Montazer-Rahmati, M. M.; Ismail, A. F.; Matsuura, T. State-of-the-Art Membrane based CO_2 Separation Using Mixed Matrix Membranes (MMMs): An Overview on Current Status and Future Directions. *Prog. Polym. Sci.* **2014**, *39*, 817−861.

(2) Lin, H.; He, Z.; Sun, Z.; Vu, J.; Ng, A.; Mohammed, M.; Kniep, J.; Merkel, T. C.; Wu, T.; Lambrecht, R. C. CO_2-Selective Membranes for Hydrogen Production and CO_2 Capture-Part I: Membrane Development. *J. Membr. Sci.* **2014**, *457*, 149−161.

(3) Ramasubramanian, K.; Zhao, Y.; Ho, W. S. W. CO_2 Capture and H_2 Purification: Prospects for CO_2-Selective Membrane Processes. *AlChE J.* **2013**, *59*, 1033−1045.

(4) Li, Y.; He, G.; Wang, S.; Yu, S.; Pan, F.; Wu, H.; Jiang, Z. Recent Advances in the Fabrication of Advanced Composite Membranes. *J. Mater. Chem. A* **2013**, *35*, 10058−10077.

(5) Robeson, L. M. Correlation of Separation Factor Versus Permeability for Polymeric Membranes. *J. Membr. Sci.* **1991**, *62*, 165−185.

(6) Robeson, L. M. The Upper Bound Revisited. *J. Membr. Sci.* **2008**, *320*, 390−400.

(7) Barankova, E.; Pradeep, N.; Peinemann, K.-V. Zeolite-Imidazolate Framework (ZIF-8) Membrane Synthesis on A Mixed-Matrix Substrate. *Chem. Commun.* **2013**, *49*, 9419−9421.

(8) Wang, S.; Liu, Y.; Huang, S.; Wu, H.; Li, Y.; Tian, Z.; Jiang, Z. Pebax-PEG-MWCNT Hybrid Membranes with Enhanced CO_2 Capture Properties. *J. Membr. Sci.* **2014**, *460*, 62−70.

(9) Liu, Y.; Peng, D.; He, G.; Wang, S.; Li, Y.; Wu, H.; Jiang, Z. Enhanced CO_2 Permeability of Membranes by Incorporating Polyzwitterion@CNT Composite Particles into Polyimide Matrix. *ACS Appl. Mater. Interfaces* **2014**, *6*, 13051−13060.

(10) Lin, R.; Ge, L.; Hou, L.; Strounina, E.; Rudolph, V.; Zhu, Z. Mixed Matrix Membranes with Strengthened MOFs/Polymer Interfacial Interaction and Improved Membrane Performance. *ACS Appl. Mater. Interfaces* **2014**, *6*, 5609−5618.

(11) Gomes, D.; Nunes, S. P.; Peinemann, K.-V. Membranes for Gas Separation based on Poly(1-trimethylsilyl-1-propyne)-Silica Nanocomposites. *J. Membr. Sci.* **2005**, *246*, 13−25.

(12) Ahn, J.; Chung, W. J.; Pinnau, I.; Song, J. S.; Du, N. Y.; Robertson, G. P.; Guiver, M. D. Gas Transport Behavior of

DOI: 10.1021/acsami.5b00106
ACS Appl. Mater. Interfaces 2015, 7, 5528−5537

Mixed-Matrix Membranes Composed of Silica Nanoparticles in a Polymer of Intrinsic Microporosity (PIM-1). *J. Membr. Sci.* **2010**, *346*, 280−287.
(13) Surya Murali, R.; Padaki, M.; Matsuura, T.; Abdullah, M. S.; Ismail, A. F. Polyaniline in Situ Modified Halloysite Nanotubes Incorporated Asymmetric Mixed Matrix Membrane for Gas Separation. *Sep. Purif. Technol.* **2014**, *132*, 187−194.
(14) Arjmandi, M.; Pakizeh, M. Mixed Matrix Membranes Incorporated with Cubic-MOF-5 for Improved Polyetherimide Gas Separation Membranes: Theory and Experiment. *J. Ind. Eng. Chem.* **2014**, *20*, 3857−3868.
(15) Zhao, Y.; Jung, B. T.; Ansaloni, L.; Ho, W. S. W. Multiwalled Carbon Nanotube Mixed Matrix Membranes Containing Amines for High Pressure CO_2/H_2 Separation. *J. Membr. Sci.* **2014**, *459*, 233−243.
(16) Cao, L.; Tao, K.; Huang, A.; Kong, C.; Chen, L. A Highly Permeable Mixed Matrix Membrane Containing CAU-1-NH_2 for H_2 and CO_2 Separation. *Chem. Commun.* **2013**, *49*, 8513−8515.
(17) Vanherck, K.; Aerts, A.; Martens, J.; Vankelecom, I. Hollow Filler based Mixed Matrix Membranes. *Chem. Commun.* **2010**, *46*, 2492−2494.
(18) Bai, H.; Li, C.; Wang, X.; Shi, G. A pH-Sensitive Graphene Oxide Composite Hydrogel. *Chem. Commun.* **2010**, *46*, 2376−2378.
(19) Li, H.; Song, Z.; Zhang, X.; Huang, Y.; Li, S.; Mao, Y.; Ploehn, H. J.; Bao, Y.; Yu, M. Ultrathin, Molecular-Sieving Graphene Oxide Membranes for Selective Hydrogen Separation. *Science* **2013**, *342*, 95−98.
(20) Zulhairun, A. K.; Ismail, A. F. The Role of Layered Silicate Loadings and Their Dispersion States on the Gas Separation Performance of Mixed Matrix Membrane. *J. Membr. Sci.* **2014**, *468*, 20−30.
(21) Du, N.; Park, H. B.; Robertson, G. P.; Dal-Cin, M. M.; Visser, T.; Scoles, L.; Guiver, M. D. Polymer Nanosieve Membranes for CO_2-Capture Applications. *Nat. Mater.* **2011**, *10*, 372−375.
(22) Galve, A.; Sieffert, D.; Staudt, C.; Ferrando, M.; Güell, C.; Téllez, C.; Coronas, J. Combination of Ordered Mesoporous Silica MCM-41 and Layered Titanosilicate JDF-L1 Fillers for 6FDA-based Copolyimide Mixed Matrix Membranes. *J. Membr. Sci.* **2013**, *431*, 163−170.
(23) Galve, A.; Sieffert, D.; Vispe, E.; Téllez, C.; Coronas, J.; Staudt, C. Copolyimide Mixed Matrix Membranes with Oriented Microporous Titanosilicate JDF-L1 Sheet Particles. *J. Membr. Sci.* **2011**, *370*, 131−140.
(24) Aroon, M. A.; Ismail, A. F.; Matsuura, T.; Montazer-Rahmati, M. M. Performance Studies of Mixed Matrix Membranes for Gas Separation: A Review. *Sep. Purif. Technol.* **2010**, *75*, 229−242.
(25) Bertelle, S.; Gupta, T.; Roizard, D.; Vallières, C.; Favre, E. Study of Polymer-Carbon Mixed Matrix Membranes for CO_2 Separation from Flue Gas. *Desalination* **2006**, *199*, 401−402.
(26) Car, A.; Stropnik, C.; Yave, W.; Peinemann, K.-V. Tailor-made Polymeric Membranes based on Segmented Block Copolymers for CO_2 Separation. *Adv. Funct. Mater.* **2008**, *18*, 2815−2823.
(27) Rahman, M. M.; Filiz, V.; Shishatskiy, S.; Abetz, C.; Neumann, S.; Bolmer, S.; Khan, M. M.; Abetz, V. PEBAX® with PEG Functionalized POSS as Nanocomposite Membranes for CO_2 Separation. *J. Membr. Sci.* **2013**, *437*, 286−297.
(28) Wang, S.; Tian, Z.; Feng, J.; Wu, H.; Li, Y.; Liu, Y.; Li, X.; Xin, Q.; Jiang, Z. Enhanced CO_2 Separation Properties by Incorporating Poly(ethylene glycol)-Containing Polymeric Submicrospheres into Polyimide Membrane. *J. Membr. Sci.* **2015**, *473*, 310−317.
(29) Li, Y.; Wang, S.; Wu, H.; Guo, R.; Liu, Y.; Jiang, Z.; Tian, Z.; Zhang, P.; Cao, X.; Wang, B. High-Performance Composite Membrane with Enriched CO_2-Philic Groups and Improved Adhesion at the Interface. *ACS Appl. Mater. Interfaces* **2014**, *6*, 6654−6663.
(30) Li, Y.; Wang, S.; He, G.; Wu, H.; Pan, F.; Jiang, Z. Facilitated Transport of Small Molecules and Ions for Energy-Efficient Membranes. *Chem. Soc. Rev.* **2015**, *44*, 103−118.
(31) Li, S.; Wang, Z.; Yu, X.; Wang, J.; Wang, S. High-Performance Membranes with Multi-Permselectivity for CO_2 Separation. *Adv. Mater. (Weinheim, Ger.)* **2012**, *24*, 3196−3200.
(32) Francisco, G. J.; Chakma, A.; Feng, X. Membranes Comprising of Alkanolamines Incorporated into Poly(vinyl alcohol) Matrix for CO_2/N_2 Separation. *J. Membr. Sci.* **2007**, *303*, 54−63.
(33) Zhao, Y.; Ho, W. S. W. CO_2-Selective Membranes Containing Sterically Hindered Amines for CO_2/H_2 Separation. *Ind. Eng. Chem. Res.* **2013**, *52*, 8774−8782.
(34) Zhao, Y.; Ho, W. S. W. Steric Hindrance Effect on Amine Demonstrated in Solid Polymer Membranes for CO_2 Transport. *J. Membr. Sci.* **2012**, *415−416*, 132−138.
(35) Zhao, S.; Wang, Z.; Qiao, Z.; Wei, X.; Zhang, C.; Wang, J.; Wang, S. Gas Separation Membrane with CO_2-Facilitated Transport Highway Constructed from Amino Carrier Containing Nanorods and Macromolecules. *J. Mater. Chem. A* **2013**, *1*, 246−249.
(36) Wu, H.; Li, X.; Li, Y.; Wang, S.; Guo, R.; Jiang, Z.; Wu, C.; Xin, Q.; Lu, X. Facilitated Transport Mixed Matrix Membranes Incorporated with Amine Functionalized MCM-41 for Enhanced Gas Separation Properties. *J. Membr. Sci.* **2014**, *465*, 78−90.
(37) Li, X.; Wang, M.; Wang, S.; Li, Y.; Jiang, Z.; Guo, R.; Wu, H.; Cao, X.; Yang, J.; Wang, B. Constructing CO_2 Transport Passageways in Matrimid® Membranes Using Nanohydrogels for Efficient Carbon Capture. *J. Membr. Sci.* **2015**, *474*, 156−166.
(38) Li, Y.; Xin, Q.; Wu, H.; Guo, R.; Tian, Z.; Liu, Y.; Wang, S.; He, G.; Pan, F.; Jiang, Z. Efficient CO_2 Capture by Humidified Polymer Electrolyte Membranes with Tunable Water State. *Energy Environ. Sci.* **2014**, *7*, 1489−1499.
(39) Bhole, Y. S.; Wanjale, S. D.; Kharul, U. K.; Jog, J. P. Assessing Feasibility of Polyarylate-Clay Nanocomposites Towards Improvement of Gas Selectivity. *J. Membr. Sci.* **2007**, *306*, 277−286.
(40) Hummers, W. S., Jr.; Offeman, R. E. Preparation of Graphitic Oxide. *J. Am. Chem. Soc.* **1958**, *80*, 1339.
(41) Lu, L. Y.; Sun, H. L.; Peng, F. B.; Jiang, Z. Y. Novel Graphite-Filled PVA/CS Hybrid Membrane for Pervaporation of Benzene/Cyclohexane Mixtures. *J. Membr. Sci.* **2006**, *281*, 245−252.
(42) Li, Y.; Wang, S.; Wu, H.; Wang, J.; Jiang, Z. Bioadhesion-Inspired Polymer-Inorganic Nanohybrid Membranes with Enhanced CO_2 Capture Properties. *J. Mater. Chem.* **2012**, *22*, 19617−19620.
(43) Car, A.; Stropnik, C.; Yave, W.; Peinemann, K.-V. PEG Modified Poly(amide-b-ethylene oxide) Membranes for CO_2 Separation. *J. Membr. Sci.* **2008**, *307*, 88−95.
(44) Lide, D. R. *CRC Handbook of Chemistry and Physics: A Ready-Reference Book of Chemical and Physical Data*; CRC Press: Cleveland, 2004.
(45) Lin, H.; Van Wagner, E.; Raharjo, R.; Freeman, B. D.; Roman, I. High-Performance Polymer Membranes for Natural-Gas Sweetening. *Adv. Mater. (Weinheim, Ger.)* **2006**, *18*, 39−44.
(46) Du, N.; Park, H. B.; Dal-Cin, M. M.; Guiver, M. D. Advances in High Permeability Polymeric Membrane Materials for CO_2 Separations. *Energy Environ. Sci.* **2012**, *5*, 7306−7322.
(47) Lin, H.; Thompson, S. M.; Serbanescu-Martin, A.; Wijmans, J. G.; Amo, K. D.; Lokhandwala, K. A.; Merkel, T. C. Dehydration of Natural Gas Using Membranes. Part I: Composite Membranes. *J. Membr. Sci.* **2012**, *413−414*, 70−81.
(48) Matteucci, S.; Yampolskii, Y.; Freeman, B. D.; Pinnau, I. *Transport of Gases and Vapors in Glassy and Rubbery Polymers*; John Wiley & Sons: New York, 2006.
(49) Wang, M.; Wang, Z.; Wang, J.; Zhu, Y.; Wang, S. An Antioxidative Composite Membrane with the Carboxylate Group as a Fixed Carrier for CO_2 Separation from Flue Gas. *Energy Environ. Sci.* **2011**, *4*, 3955−3959.
(50) Wang, Z.; Li, M.; Cai, Y.; Wang, J. X.; Wang, S. C. Novel CO_2 Selectively Permeating Membranes Containing PETEDA Dendrimer. *J. Membr. Sci.* **2007**, *290*, 250−258.
(51) Du, J. R.; Liu, L.; Chakma, A.; Feng, X. A Study of Gas Transport Through Interfacially Formed Poly(N,N-dimethylaminoethyl methacrylate) Membranes. *Chem. Eng. J.* **2010**, *156*, 33−39.
(52) Francisco, G. J.; Chakma, A.; Feng, X. Separation of Carbon Dioxide from Nitrogen Using Diethanolamine-Impregnated Poly(vinyl alcohol) Membranes. *Sep. Purif. Technol.* **2010**, *71*, 205−213.

DOI: 10.1021/acsami.5b00106
ACS Appl. Mater. Interfaces 2015, 7, 5528−5537